

1 **Impact of the Electric Field Variability on the Joule heating**
2 **and thermosphere**

Yue Deng, Astrid Maute, Arthur D. Richmond and Raymond G. Roble

3 High Altitude Observatory, National Center for the Atmospheric Research,

4 Boulder Colorado, U.S.A.

Yue Deng (e-mail: ydeng@ucar.edu), Astrid Maute (e-mail: maute@ucar.edu), Arthur D. Richmond
(e-mail: richmond@ucar.edu), Raymond G. Roble (e-mail: roble@ucar.edu).

Abstract.

A new quantitative empirical model of the high-latitude forcing of the thermosphere, which is the first empirical model with an electric field variability component consistent with the average electric field, is used with the NCAR-TIEGCM to investigate the influence of the electric field variability on the Joule heating, neutral temperature and density. The electric field variability increases the Joule heating by more than 100%, and significantly improves the agreement between the total Joule heating and Poynting flux, while the horizontal distributions of the height-integrated Joule heating and the Poynting flux have some detailed differences in the polar cap and nightside regions. Including the electric field variability into the energy calculation results in significant changes in the neutral temperature and density. At 400 km, it causes a 120 K polar average temperature increase and the corresponding percentage difference of density is close to 30%.

1. Introduction

19 The thermosphere/ionosphere is forced by solar EUV radiation, high-latitude electrody-
20 nics, particle precipitation and waves propagating from the lower atmosphere. In the polar re-
21 gion, field-aligned currents from the magnetosphere are closed by ionospheric currents, and
22 bring a significant amount of energy into the thermosphere/ionosphere. The energy is highly
23 variable with the geomagnetic conditions and can cause global scale disturbances in the ther-
24 mosphere/ionosphere during a storm period. However, this energy has usually been underes-
25 timated when the general circulation models (GCMs) are driven by climatological convection
26 models. For example, *Emery et al.* [1999] needed to multiply the calculated Joule heating by
27 2.5 in the winter hemisphere in order to reproduce observed thermospheric responses. This in-
28 sufficient energy is attributed to the neglect of the contribution of electric field variability to the
29 Joule heating [*Codrescu et al.*, 1995]. Using the ion drift data from the Millstone Hill radar,
30 *Codrescu et al.* [1995] reported that the electric field variability has a similar magnitude as the
31 average electric field. Indeed, subsequent studies [*Codrescu et al.*, 2000; *Matsuo et al.*, 2003;
32 *Matsuo and Richmond*, 2008; *Golovchanskaya*, 2008] showed that the electric field variability
33 can be comparable to or even larger than the average electric field.

34 While the significance of electric field variability to the Joule heating has been recognized, we
35 still face a big challenge to implement the electric field variability in the GCMs appropriately
36 and conveniently. Empirical models have been developed to characterize the auroral precipita-
37 tion and high-latitude electric potential under various geophysical conditions, which are often
38 used to force GCMs. However, the models of the electric potential represent only the statistical
39 average of the vector field $\langle \mathbf{E} \rangle$, and the difference between \mathbf{E} and $\langle \mathbf{E} \rangle$, called “residual electric

40 field”, has been ignored. To quantify the Joule heating associated with the residual electric field
41 in a way consistent with the empirical model of electric potential used as GCM inputs, a new
42 empirical model with an electric field variability component has been developed and coupled
43 with the NCAR-TIEGCM [Roble *et al.*, 1988; Richmond *et al.*, 1992], which supplies a more
44 realistic way to include electric field variability in the energy estimation than through ad hoc
45 increases to the Joule heating. In this paper, we compare the thermospheric responses to the
46 Joule heating calculated either from an empirical model of electric potential, or from both this
47 potential and the empirical model of electric field variability. The resulting energy inputs then
48 have been validated with the empirical model of Poynting flux. Including the electric field vari-
49 ability significantly improves consistency between the Joule heating and Poynting flux, and the
50 corresponding neutral temperature and density increase substantially.

2. Empirical Model of the High Latitude Forcing

51 Dynamic Explorer 2 (DE-2) is one of only a few spacecraft that measured simultaneously
52 the electric and magnetic fields, ion velocities, and particle precipitation at low-Earth orbit. By
53 analyzing observations from the DE-2 spacecraft, a comprehensive, mutually consistent model
54 of high-latitude thermospheric forcing has been developed and will be detailed in a separate
55 paper [Richmond and Maute, 2009]. Totally, 2895 satellite passes during August 1981-March
56 1983 have been used in the process. The cross-track ion drift measurements are from the Ion
57 Drift Meter (IDM), the along-track ion drift measurements are from the Retarding Potential
58 Analyzer (RPA), and the magnetic field measurements are from the Fluxgate Magnetometer
59 (MAGB). The electric field \vec{E} is calculated as $-\vec{V} \times \vec{B}$, where \vec{V} is the ion velocity in the
60 Earth frame and \vec{B} is the geomagnetic field. A magnetic perturbation field $\Delta\vec{B}$ is obtained by

61 subtracting a main-field model from the observations, and then correcting for spacecraft attitude
 62 uncertainties by subtracting a straight-line baseline that goes to zero at $\pm 45^\circ$ magnetic latitude.
 63 The observations were fitted, at each magnetic latitude, to analytical functions of magnetic local
 64 time (MLT), dipole tilt angle with respect to the plane normal to the Sun-Earth line, and strength
 65 and clock angle of the interplanetary magnetic field (IMF) obtained from the IMP 8 and ISEE
 66 3 satellites measurements. Currently, the empirical model includes four components: electric
 67 potential, magnetic potential, electric field variability and Poynting flux. A consistent auroral
 68 particle precipitation model will be developed in the future through analyzing the ion / electron
 69 energy flux data from the Low Altitude Plasma Instrument (LAPI).

70 The resultant electric and magnetic potentials from the new empirical model are generally
 71 consistent with those of *Weimer* [2005], which were derived from the along-track components of
 72 electric and magnetic fields. The downward Poynting flux S_{down} at the top of the thermosphere
 73 is estimated using the combined ion-drift and magnetometer data. In this model, the Poynting
 74 flux is calculated from the point measurements of electric field and magnetic field data from
 75 the DE-2 satellite, and is then fitted to analytical functions in a similar manner to the electric
 76 and magnetic potentials. The resultant model is similar to the average of the product of \mathbf{E} and
 77 $\Delta \mathbf{B}$ ($\frac{\langle \mathbf{E} \times \Delta \mathbf{B} \rangle}{\mu_0}$), which at some level includes the contribution of the electric field variability.
 78 In contrast, the *Weimer* [2005] model calculates the Poynting flux from the product of average
 79 \mathbf{E} and $\Delta \mathbf{B}$ as $\frac{\langle \mathbf{E} \rangle \times \langle \Delta \mathbf{B} \rangle}{\mu_0}$, which is smaller than that from the new empirical model due to the
 80 neglect of the small-scale variability. Our model of electric field variability is the root mean
 81 square (RMS) of the difference between the DE-2 observations E^{DE2} and the electric field
 82 E^{model} obtained from the electric potential model:

$$\sigma(E) = \sqrt{\frac{\sum_{i=1}^N (E_i^{DE2} - E_i^{model})^2}{N}}, \quad (1)$$

83 where the subscript i is for individual measurements, N is number of measurements, and where
 84 σ is calculated separately for the eastward and poleward components of \vec{E} . Since the electric
 85 field variability represents the difference between the DE-2 observation and empirical average
 86 model, it includes both small- and large-scale spatial variations, as well as temporal variations.
 87 The patterns and magnitudes of the electric-field variability, not shown here, are comparable
 88 with those shown by *Matsuo et al.* [2003]. This is the first empirical model in the community
 89 which includes a electric field variability component consistent with the average electric field.

3. Results

90 To investigate the importance of electric field variability to the Joule heating, we have cou-
 91 pled the new high-latitude forcing model into the TIEGCM. Figure 1a shows the distribution
 92 of the altitude-integrated Joule heating from an equinox simulation in the northern hemisphere,
 93 when the empirical electric potential from the new forcing model has been used to drive the ion
 94 drift. The IMF conditions are $B_y = 0$ and $B_z = -5nT$. The hemispheric power of precip-
 95 itating auroral particles is 30 GW, and $F_{10.7}$ is $150 \times 10^{-22} W/m^2 Hz$. Figure 1b is the same
 96 as Figure 1a, except that the electric field variability from the empirical forcing model has also
 97 been implemented in the TIEGCM. The electric field variation is used by alternating the sign of
 98 the electric field standard deviation from the model for a given point at every time step in both
 99 the north-south and east-west directions. This methodology easily saturates the required stan-
 100 dard deviation and zero average conditions, and the assumption is that the variation is spatially
 101 full-correlated and temporally un-correlated, which is consistent the characteristic of the small-

102 scale variation shown in *Matsuo and Richmond* [2008]. Comparison between Figures 1a and 1b
103 shows that the electric field variability increases the Joule heating significantly. For example, the
104 maximum at dawn and dusk increases from 0.009 to 0.018 W/m^2 . To derive Joule heating from
105 GCMs requires additional accurate information about the instantaneous patterns of ionospheric
106 conductivities and thermospheric winds. The estimates of height-integrated Joule heating need
107 to be calibrated against techniques less subject to bias, like the estimation of Poynting flux. Fig-
108 ure 1c shows the Poynting flux at the top of the thermosphere from the new empirical model,
109 which has a larger energy input on the dayside than in the midnight, and is different from the
110 aurora particle precipitation. Both Figures 1b and 1c show dawn and dusk peaks with similar
111 magnitudes, and a large energy flux in the dayside cusp region. But the Poynting flux is larger
112 in the polar cap and smaller on the night side than the Joule heating calculated with the average
113 electric field and electric field variability.

114 Figure 2 shows the hemispherically integrated Joule heating in the northern hemisphere from
115 TIEGCM simulations and Poynting flux from the new empirical model in different seasons.
116 The difference between the green columns and dark blue columns is more than 100%, which
117 indicates the electric field variability has a comparable contribution to the Joule heating as the
118 average electric field. The light blue columns represent the integrated Poynting flux from the
119 new empirical model. Clearly, the calculated Joule heating with the average electric field and
120 electric field variability is much closer to the Poynting flux than that using only the average
121 electric field. Generally, the electric field variability strongly improves the agreement between
122 Joule heating and Poynting flux. In summer and winter seasons, the calculated total Joule
123 heating is larger than the Poynting flux, which is not physical because the generation of wind

124 kinetic energy by the Lorentz force of the current has a small positive value (not shown), and
125 Poynting flux is equal to the sum of Joule heating and Kinetic-energy generation. This may
126 be caused in part by inconsistency between the conductivity and the electric field when the
127 Joule heating is calculated in the TIEGCM. In the future, the empirical model will also include
128 a consistent particle precipitation part, which may help to make the patterns of conductivity
129 and electric field more consistent. The Joule heating calculated with the average electric field
130 in summer is larger than that in winter, which is similar to the seasonal variation of the Joule
131 heating shown in *Weimer* [2005]. *Matsuo et al.* [2003] presented a clear seasonal dependence of
132 the electric field variability, with a maximum in winter and minimum in summer. However, in
133 our study the energy contribution of electric field variability, which is indicated by the absolute
134 value difference between the dark blue and green columns in Figure 2, has no clear seasonal
135 dependence. This is because the conductance is largest in summer and smallest in winter, which
136 is opposite to the seasonal variation of electric field variability.

137 Figure 3a shows the polar average (poleward 47.5°) thermospheric temperature profiles with
138 different high-latitude energy inputs in the equinox season. The difference between the case in
139 which only the average electric field is used in the Joule heating calculation (black) and the case
140 in which both the average electric field and electric field variability are used (red) is close to
141 120 K above 300 km altitude. *Fesen et al.* [1997] reported that the TIEGCM simulated neutral
142 temperature is 100-200 K lower than the Millistone Hill observation at 300 km for the January
143 1993 campaign and it was proposed that the discrepancy was due to the underestimate of Joule
144 heating caused by the electric field variability. The similarity between the temperature differ-
145 ence shown in this study and that presented in *Fesen et al.* [1997] indicates that including the

146 electric field variability will improve the agreement between observations and simulations. Fig-
147 ure 3b shows the distribution of temperature difference between the two cases with and without
148 electric field variability at 400 km altitude. The temperature difference is positive in the whole
149 polar region, and the maximum difference is 250 K in the dawnside and the minimum is close to
150 62 K at lower latitudes. Interestingly, there is no clear relation between the patterns of temper-
151 ature and height-integrated heating, due to the fact that dynamics has a major influence on the
152 temperature. As a reference, the blue line in Figure 3a shows the temperature profile obtained
153 when the Poynting flux from the new empirical model has been used to specify the energy input
154 from the magnetosphere. Since the Poynting flux model contains no information about the alti-
155 tudes where the electromagnetic energy is deposited, the energy has been distributed vertically
156 as heat according to the Pederson conductivity [Deng *et al.*, 2008]. In Figure 3a, the red line is
157 closer to the blue line than to the black line, and the difference between the red and blue lines
158 is close to 50 K above 300 km, which is related to the total energy difference between Joule
159 heating and Poynting flux for the equinox case shown in Figure 2 .

160 Figure 3c shows the density percentage difference compared with the case in which the Joule
161 heating is calculated with the average electric field. When the Joule heating is calculated in-
162 cluding the electric field variability (red), the polar-average density increases by 30% at 400 km
163 altitude. Figure 3d shows that the maximum density percentage difference goes to more than
164 70% in the dawn cell and the minimum is above 15% on the dayside at 400 km. The density dif-
165 ference is significant and comparable with the density disturbance observed by CHAMP during
166 a moderate geomagnetic storm. Clearly, the variations of density and temperature have differ-
167 ent patterns. One possible reason is that Figure 3b shows the value difference of temperature

168 and Figure 3d shows the percentage difference of density. Meanwhile, the horizontal convec-
169 tion, as well as the vertical atmospheric expansion and contraction caused by the variation of
170 temperature, can change the density distribution significantly.

4. Summary and Conclusion

171 The significance of electric field variability to the Joule heating has been pointed out by
172 *Codrescu et al.* [1995] and subsequent studies, but it is still very challenging to include the elec-
173 tric field variability in the GCMs appropriately and conveniently. A new quantitative empirical
174 model of the high-latitude forcing of the thermosphere, including electric potential, electric field
175 variability and Poynting flux, is coupled with the NCAR-TIEGCM to investigate the influence
176 of the electric field variability on the Joule heating, neutral temperature and density.

177 In the TIEGCM simulations, the Joule heating has been calculated with and without the elec-
178 tric field variability. The integrated Joule heating has been validated with the Poynting flux
179 from the empirical model. The analysis reveals that the electric field variability increases the
180 Joule heating by more than 100%, and significantly improves the consistency between the Joule
181 heating and Poynting flux, while their horizontal distributions have some detailed differences in
182 the polar cap and nightside regions.

183 Including the electric field variability into the energy calculation results in significant changes
184 to the neutral temperature and density. For example, it causes a 120 K polar average exospheric
185 temperature increase at 400 km ranging from 62 K to 250 K. The corresponding percentage
186 difference of density is close to 30% for the polar average, and localized differences can be 16%
187 to 75%.

References

- 188 Codrescu, M. V., T. J. Fuller-Rowell, and J. C. Foster, On the importance of E-field variability
189 for Joule heating in the high-latitude thermosphere, *Geophys. Res. Lett.*, *22*, 2393, 1995.
- 190 Codrescu, M. V., T. J. Fuller-Rowell, J. C. Foster, J. M. Holt, and S. J. Cariglia, Electric field
191 variability associated with the Millstone Hill electric field model, *J. Geophys. Res.*, *105*, 5265,
192 2000.
- 193 Deng, Y., A. Maute, A. D. Richmond, and R. G. Roble, Analysis of thermospheric response
194 to magnetospheric inputs, *Journal of Geophysical Research (Space Physics)*, *113*, doi:
195 10.1029/2007JA012840, 2008.
- 196 Emery, B. A., C. Lathuillere, P. G. Richards, R. G. Roble, M. J. Buonsanto, D. J. Knipp,
197 P. Wilkinson, D. P. Sipler, and R. Niciejewski, Time dependent thermospheric neutral re-
198 sponse to the 2-11 November 1993 storm period, *Journal of Atmospheric and Terrestrial*
199 *Physics*, *61*, 329–350, 1999.
- 200 Fesen, C. G., B. A. Emery, M. J. Buonsanto, Q. H. Zhou, and M. P. Sulzer, Simulations of
201 the F region during the January 1993 10-day campaign, *J. Geophys. Res.*, , *102*, 7249–7266,
202 doi:10.1029/96JA03312, 1997.
- 203 Golovchanskaya, I. V., Assessment of Joule heating for the observed distributions of high-
204 latitude electric fields, *Geophys. Res. Lett.*, , *35*, 16,102, doi:10.1029/2008GL034413, 2008.
- 205 Matsuo, T., and A. D. Richmond, Effects of high-latitude ionospheric electric field variabil-
206 ity on global thermospheric Joule heating and mechanical energy transfer rate, *Journal of*
207 *Geophysical Research (Space Physics)*, *113*, 7309, doi:10.1029/2007JA012993, 2008.

- 208 Matsuo, T., A. D. Richmond, and K. Hensel, High-latitude ionospheric electric field variability
209 and electric potential derived from DE-2 plasma drift measurements: Dependence on IMF
210 and dipole tilt, *J. Geophys. Res.*, *108*, 1005, 2003.
- 211 Richmond, A. D., and A. Maute, A new empirical model of the high latitude forcing , *Journal*
212 *of Geophysical Research (Space Physics)*, p. In preparation, 2009.
- 213 Richmond, A. D., E. C. Ridley, and R. G. Roble, A thermosphere/ionosphere general circulation
214 model with coupled electrodynamics, *Geophys. Res. Lett.*, *19*, 369, 1992.
- 215 Roble, R. G., E. C. Ridley, A. D. Richmond, and R. E. Dickinson, A coupled ther-
216 mosphere/ionosphere general circulation model, *Geophys. Res. Lett.*, *15*, 1325, 1988.
- 217 Weimer, D. R., Improved ionospheric electrodynamic models and application to calculat-
218 ing Joule heating rates, *Journal of Geophysical Research (Space Physics)*, *110*, 5306, doi:
219 10.1029/2004JA010884, 2005.

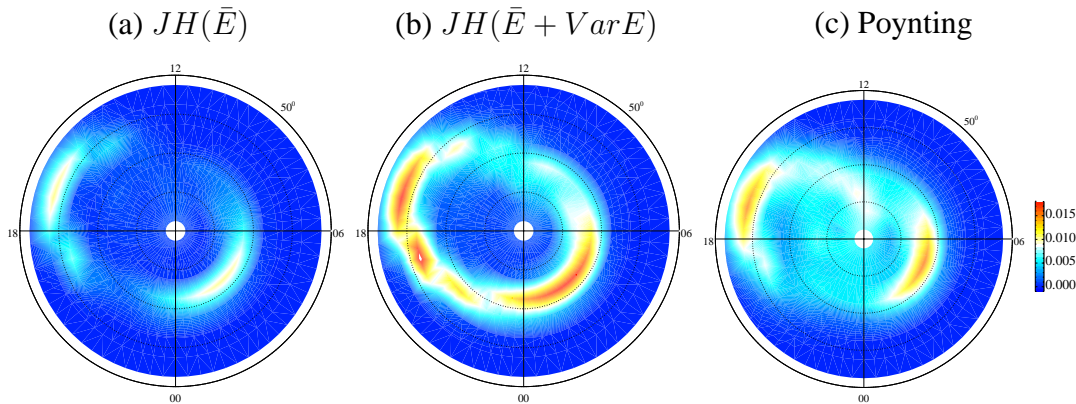


Figure 1. (a) Distribution of the altitude-integrated Joule heating (W/m^2) in the northern hemisphere in equinox from a TIEGCM simulation, when the average electric field is used in the Joule heating calculation. The IMF conditions are $B_y = 0$ and $B_z = -5nT$. The hemispheric power is 30 GW and $F_{10.7}$ is $150 \times 10^{-22} W/m^2 Hz$. Geographic coordinates are used in this figure. (b) Same as (a), but the electric field variability from the empirical model is also included in the calculation. (c) Poynting flux at the top of the thermosphere from the empirical model.

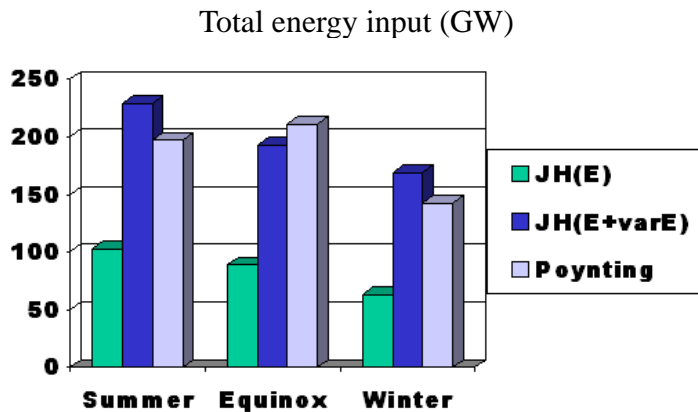


Figure 2. Hemispherically integrated Joule heating in the northern hemisphere from TIEGCM simulations and Poynting flux from the empirical model in different seasons. The green columns are for the case in which the average electric field is used in the Joule heating calculation. The dark blue columns are for the case in which both average electric field and electric field variability are included in the calculation. The light blue columns represents the integrated Poynting flux from the empirical model.

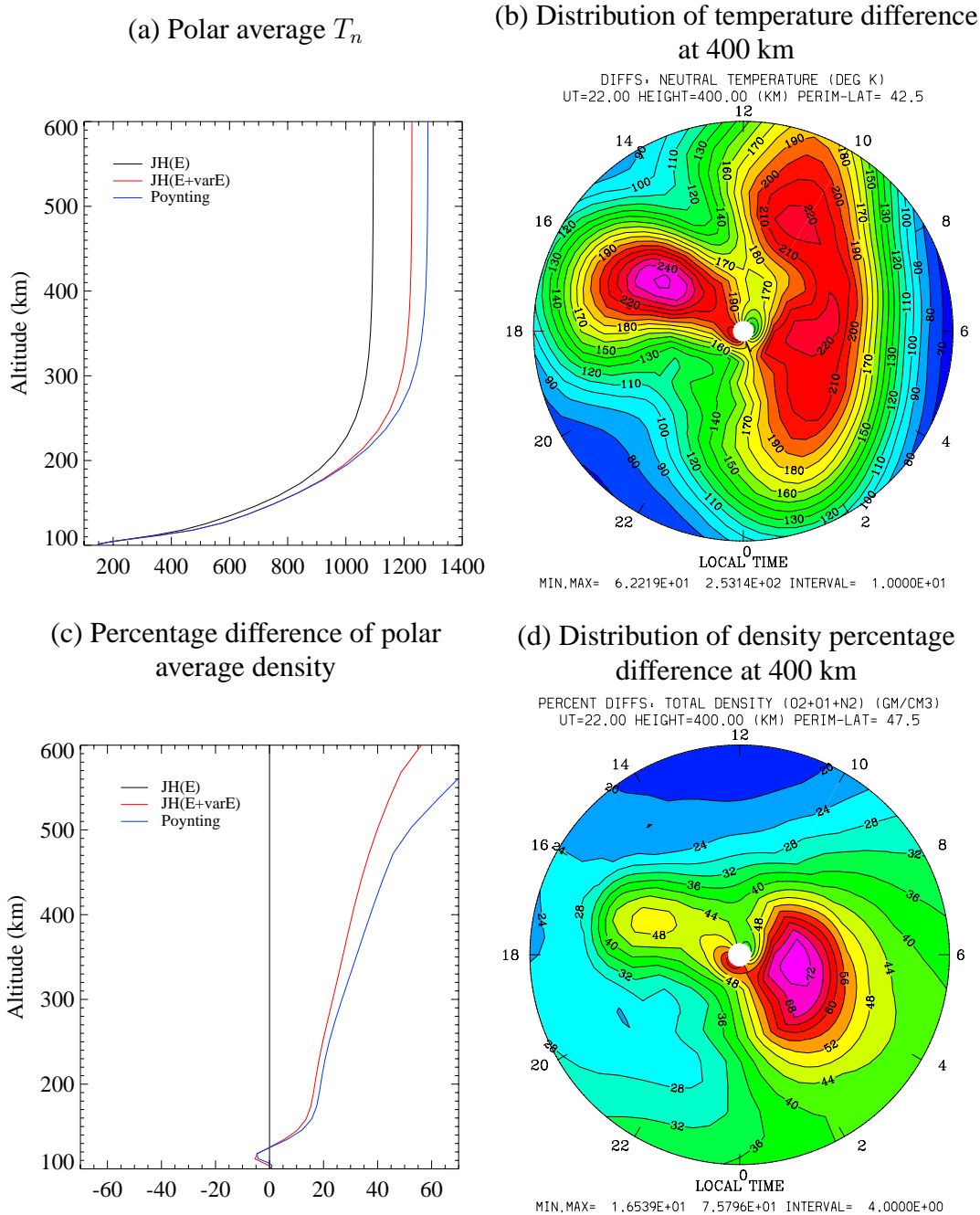


Figure 3. (a) Polar average (poleward 47.5°) thermospheric temperature profiles at equinox with different high-latitude energy inputs. The black line is for the case in which Joule heating is calculated with the average electric field. The red line is for the case in which both the average electric field and electric field variability are included in the Joule heating calculation. The blue line is for the case in which the energy input is specified by the Poynting flux from the empirical model (see text). (b) Distribution of temperature difference between the cases with and without the electric field variability at 400 km altitude. (c) Percentage difference of the polar average (poleward 47.5°) thermospheric density compared with the average electric field case. The black line at zero is for the case in which Joule heating is calculated with the average electric field. The red line is for the case in which both the average electric field and electric field variability are included in the Joule heating calculation. The blue line is for the case in which the energy input is specified by the Poynting flux from the empirical model. (d) Distribution of percentage density difference between the cases with and without the electric field variability at 400 km altitude.